ELSEVIER

Thermochimica Acta 379 (2001) 7–14

thermochimica acta

www.elsevier.com/locate/tca

Calorimetric study on NH_3 insertion reaction into microporous manganese oxides with (2×2) tunnel and $(2 \times \infty)$ layered structures

Z.-M. Wang*, H. Kanoh[1]

Aquamaterial Separation Technology RG, Marine Resources and Environment Institute (MRE), National Institute of Advanced Industrial Science and Technology (AIST) 2217-14 Hayashi-cho, Takamatsu-shi, Kagawa 761-0395, Japan

Abstract

NH_3 insertion mechanism into the (2×2) tunnel structure of a hollandite-type manganese oxide (H-Hol) and the $(2 \times \infty)$ layered structure of a birnessite-type manganese oxide (H-Bir) were studied by direct adsorption calorimetry. It was found that H-Bir has a smaller NH_3 adsorption enthalpy ($-\Delta H_{d,NH_3}$) compared to H-Hol because of the structural flexibility of its MnO sheets. NH_3 insertion into the tunnel structure of H-Hol is divided into two stages: in the initial stage, NH_3 molecules interact with the H^+ sites at the external surfaces and near the tunnel entrance, giving a peak in $-\Delta H_{d,NH_3}$ curve at a low adsorption temperature due to the energy barrier required to expand the lattice structure; in the secondary stage, NH_3 can access the inner H^+ sites in the tunnel, giving a broad shoulder in $-\Delta H_{d,NH_3}$ curve. H_2O/H^+ contents in H-Hol have an important role in NH_3 insertion. Porous manganese oxides have a comparable or much higher $-\Delta H_{d,NH_3}$ value compared to zeolites having a similar pore dimension or of a same proton form.

Keywords: Microcalorimetry; NH_3; Adsorption; Micropore; Manganese oxide

1. Introduction

As one group of hopeful porous transition metal oxides, porous manganese oxides have recently received extensive attention because of their multi-functional roles as cathode materials for rechargeable batteries [1–4] and ion-sieving adsorbents [5–8]. Generally speaking, porous manganese oxides are constructed of regularly arranged MnO_6 octahedral units, containing one-dimensional tunnel or layered micropores with sizes below 1 nm [9,10]. Hollandite- and birnessite- type manganese oxides have the (2×2) tunnel structure and $(2 \times \infty)$ layered structure, respectively, as shown in Fig. 1. Since the various valences of lattice manganese result in a negative skeleton, counter cations can be inserted in between the microporous structure. This property holds the promise of applications for cation insertion in rechargeable batteries or cation exchange from the liquid phase on the one hand, but restricts entry of gas probes in a process of gas phase adsorption or reaction on the other hand. Manganese oxides, both bulk and supported, can be the active species for many heterogeneous catalytic reactions such as ozone decomposition, selective NO_x reduction, etc. [10–15]. However,

* Corresponding author. Tel.: +81-87-869-3574; fax: +81-87-869-3550.
E-mail addresses: zmwang@aist.go.jp (Z.-M. Wang), kanoh@pchem2.s.chiba-u.ac.jp (H. Kanoh).
[1] Department of Chemistry, Faculty of Science, Chiba University, 1-33 Yayoi-cho, Inage-ku, Chiba 263-8522, Japan.

0040-6031/01/$ – see front matter
PII: S0040-6031(01)00596-2

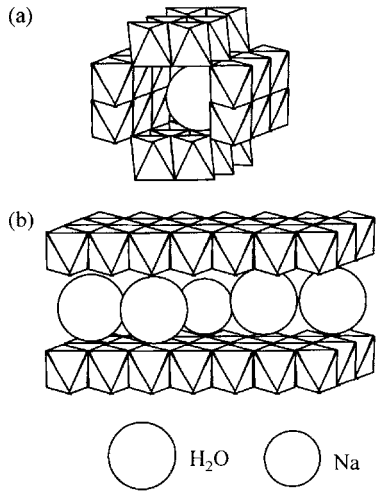

Fig. 1. A (2×2) tunnel structure of hollandite and $(2 \times \infty)$ layered structure of birnessite.

research on gas adsorption/reaction of porous manganese oxides themselves is so far limited.

Recently, the authors found that NH_3 molecules can be selectively inserted into the tunnel structure of a hydrous hollandite-type manganese oxide (H-Hol) even in the presence of water [16,17]. The inserted NH_3 molecules can be decomposed into nitrogen accompanied by destruction of the crystal structure on rising desorption temperature, indicating a possible application of H-Hol as a selective killer for odor NH_3. On the other hand, birnessite-type manganese oxide (H-Bir) can be easily intercalated by alkylammonium ions, from which a new type of SiO_2-pillared manganese oxide with open micropores has been derived [18]. In this study, the insertion mechanism of NH_3 into micropores of hollandite- and birnessite-type manganese oxides was examined using direct adsorption microcalorimetry. An unusual phenomenon for NH_3 insertion into (2×2) tunnel structure of H-Hol is reported and the results will be compared with aluminosilicate crystals such as A-type zeolite and proton-type mordenite.

2. Experimental

2.1. Materials and start

H-Hol was synthesized by a hydrothermal reaction of an Li_2MnO_3 precursor in a 3 M sulfuric acid solution at 363 K for 48 h [19]. The Li_2MnO_3 precursor was prepared by calcining the mixture of MnOOH and Li_2CO_3 at 1073 K for 48 h. The H-Hol product was dialyzed against distilled water for 3 days to remove sulfate ions and dried at 343 K for one night before use. A potassium type of hollandite manganese oxide (K-Hol) was obtained by immersing the H-Hol sample in 3 M KOH solution for one day, successive washing with distilled water and drying in air at 343 K for one night. Birnessite-type manganese oxide was prepared by the method reported in the literature [18]. A mixed solution of 0.6 M NaOH and 2 M H_2O_2 was poured quickly into a 0.3 M $Mn(NO_3)_2$ solution and stirred for 25 min. The precipitate was then subjected to hydrothermal treatment at 150°C for 16 h in a 2 M NaOH solution. The obtained precipitates (Na-form binessite-type oxide) were treated with a 0.1 M HCl solution at room temperature for 3 days to produce a proton type (H-Bir). A typical chemical formula of H-Bir is $Na_{0.21}H_{3.49}Mn_{12}O_{23}{\cdot}9.5H_2O$. A Linde A-type zeolite (3A) with a similar pore opening to those of H-Hol and H-Bir and a H-type mordenite (H-Mor) with a chemical formula of $Na_{0.06}H_{0.34}Al_{0.4}Si_{47.6}O_{96}$ was supplied from Toso Co. Ltd. All the samples were preserved in a dessicator under humidity control below 20%.

2.2. XRD and TG/DTA measurements

The X-ray diffraction (XRD) patterns of the samples were measured by a Rigaku RINT 1200 diffractometer which has a Cu Kα emission ($\lambda = 0.15405$ nm) and a graphite monochromator. The measurement was carried out from 5 to 70° at a scanning speed of 0.02°/min in a humidity/temperature controllable chamber. The lattice constants of H-Hol before and after NH_3 adsorption were calculated from diffraction parameters of (1 1 0), (2 0 0), (3 1 0) and (2 1 1) planes. The basal plane departures of H-Bir before and after NH_3 adsorption were calculated from the diffraction parameters of (0 0 2) plane.

10 mg of the grounded samples, which were preserved in a dessicator, were immediately weighed in air, placed in a platinum vessel, and then subjected to TG/DTA (Mac Science Co. Ltd., TG/DTA 2000) measurement from room temperature to 1273 K at a ramp rate of 10 K/min in a curtain gas flow (air, 100 ml/min). Commercial α-Al_2O_3 powders were used as the reference solid.

2.3. Microcalorimetric measurement

NH_3 differential adsorption enthalpies on the zeolites and manganese oxides were measured at 323 or 393 K by a Tian–Calvet type heat-flow calorimeter (Tokyo Riko Co., HAC-450G). The calorimeter is equipped with a standard volumetric adsorption–desorption device having a MKS-made pressure transducer and an automatic NH_3 injection system. The 3A and H-Mor were pre-evacuated at 623 and 823 K, respectively, for 3 h, and the porous manganese oxides at the required temperatures for 2 h prior to microcalorimetric measurement.

3. Results

3.1. XRD and TG/DTA results

XRD results showed that 3A and H-Mor have the correct crystal structures of typical Linde-A and mordenite types, respectively [20]. H-Hol and K-Hol have the same structure of natural cryptomelane type [21] except for a smaller diffraction angle for K-Hol due to a larger ionic radius of K^+ (0.138 nm). The rectangular tunnel structure of H-Hol is held together by linked MnO_6 octahedral units with small H^+ and H_2O filled inside. The lattice constants of H-Hol and K-Hol are determined as $a = b = 0.975$ and 0.979 nm, and $c = 0.285$ and 0.285 nm, respectively. In contrast, H-Bir has a layered structure constructed of stacked planes of MnO_6 octahedral assembly with a basal spacing of 0.729 nm.

Fig. 2 shows the TG/DTA curves of H-Hol, K-Hol and H-Bir. On increasing temperature, H-Hol exhibits a gradual dehydration until 673 K, followed by two step-wise weight losses at 800 and 1188 K, which correspond to two endothermic peaks in DTA curves due to the transformation of α-MnO_2 to Mn_2O_3 and of Mn_2O_3 to Mn_3O_4, respectively. In comparison with H-Hol, K-Hol exhibits less dehydration below 773 K and a smaller weight loss step at 870 K due to the structural change from α-MnO_2 to Mn_2O_3. On the other hand, H-Bir has three evident steps for dehydration: a step at the lower temperature range (<523 K) and the steps at 823 and 1065 K. Fig. 3 shows the XRD patterns of H-Bir after evacuation at various temperatures. The framework structure of H-Bir can be easily

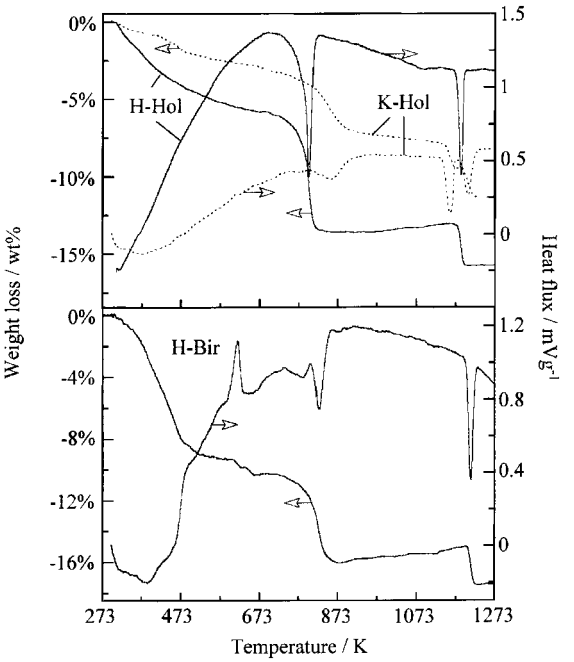

Fig. 2. TG/DTA curves of H-Hol, K-Hol and H-Bir.

destructed on heating above 373 K. On the other hand, the crystal structure of H-Hol is not changed by heating in vacuum at a temperature as high as 673 K, as confirmed by other research [22]. The layer

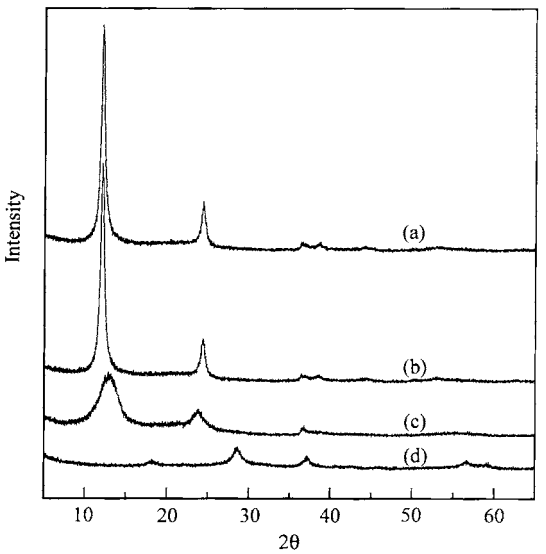

Fig. 3. XRD patterns of H-Bir after evacuation for 1 h at (a) 323, (b) 343, (c) 373 and (d) 573 K.

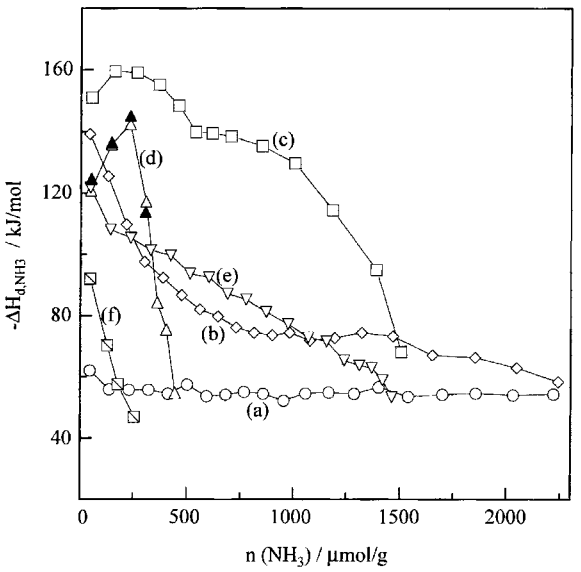

Fig. 4. NH_3 differential adsorption enthalpy at 323 K on (a) 3A, (b) H-Mor, (c)H-Hol-323, (d) K-Hol-393, (e) H-Bir-323, (f) H-Bir-473. The solid mark denotes the second measurement and the values after H-Hol and H-Bir are the pre-evacuation temperatures.

structure of H-Bir contains plenty of water which stabilizes the crystal structure of H-Bir by balancing the electrostatic MnO layers with strong hydrogen bonding or electrostatic interaction energy [23].

3.2. Microcalorimetric results

Fig. 4 shows the changes of NH_3 differential enthalpy ($-\Delta H_{d,NH_3}$) at 323 K on various zeolites and porous manganese oxides. The $-\Delta H_{d,NH_3}$ value on 3A is almost constant in the whole adsorption range, indicating no specific interaction between NH_3 and the zeolite surface. The overlapping of potential fields of uniform micropore walls of 3A enhances the interaction of NH_3 with the pore walls, giving an adsorption energy with 35 kJ/mol greater than the NH_3 liquefaction enthalpy ($-\Delta H_{L,liq} =$ 19.9 kJ/mol at 298 K [24]). $-\Delta H_{d,NH_3}$ on H-Mor has a heterogeneous property with a much higher value than that on 3A due to the strong interaction with the surface acidic sites [25]. $-\Delta H_{d,NH_3}$ of H-Bir is also of heterogeneous property; its changing curve crosses that of H-Mor, having a smaller value at the initial part and a larger value at $n(NH_3) = 260$–1000 μmol/g. Destruction of the crystal structure of

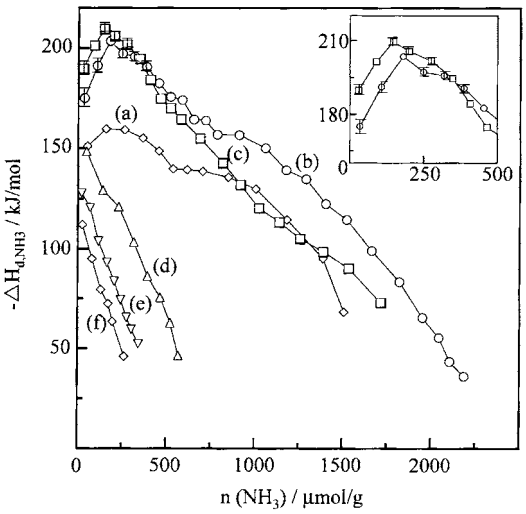

Fig. 5. NH_3 differential adsorption enthalpy at 323 K on H-Hol after evacuation at (a) 323, (b) 393, (c)473, (d) 573, (e) 673 and (f) 773 K.

H-Bir brings about the loss of NH_3 adsorption sites (Fig. 4f). In comparison with H-Bir and the zeolite samples, H-Hol possesses a much higher $-\Delta H_{d,NH_3}$ value over a wide NH_3 adsorption range. There is a broad peak in the $-\Delta H_{d,NH_3}$ curve on H-Hol at the initial NH_3 adsorption stage and a broad shoulder at the higher NH_3 adsorption, indicating that two successive adsorption processes exist for NH_3 insertion into the tunnel structure of H-Hol. The $-\Delta H_{d,NH_3}$ curve on K-Hol reveals a sharp peak at low NH_3 adsorption, whose position coincides with the first broad peak of that on H-Hol, in spite of a small total NH_3 adsorption with $-\Delta H_{d,NH_3} > 50$ kJ/mol.

Fig. 5 shows the relationship between the $-\Delta H_{d,NH_3}$ value at 323 K and the pre-evacuation temperature of H-Hol. On increasing the evacuation temperature until 473 K, the interaction between NH_3 and H-Hol becomes stronger, revealing a much higher $-\Delta H_{d,NH_3}$ value in the whole adsorption range. Especially, the interaction energy of NH_3 with H-Hol is greatly enhanced at NH_3 adsorption below 600 μmol/g, producing more evident peaks in this range, which are as sharp as that on K-Hol. The broad shoulder of the $-\Delta H_{d,NH_3}$ curve at higher NH_3 adsorption is still present, having a higher $-\Delta H_{d,NH_3}$ value under evacuation at 393 K, but becomes less evident under evacuation at 473 K. Evacuation at 473 K slightly enhances the $-\Delta H_{d,NH_3}$ values before the first peak

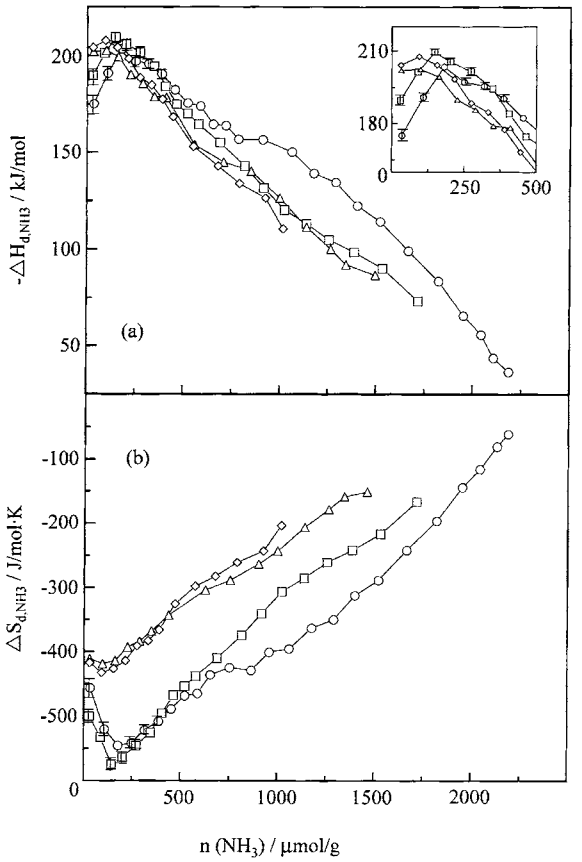

Fig. 6. Comparison of (a) NH_3 differential adsorption enthalpy (b) NH_3 differential entropy at 323 and 393 K on H-Hol. (○, □): at 323 K after evacuation at 393 and 473 K, respectively; (△), (◇): at 393 K after evacuation at 393 and 473 K, respectively.

at the low NH_3 adsorption in comparison with those under evacuation at 393 K. On the other hand, the $-\Delta H_{d,NH_3}$ values are gradually decreased with increasing evacuation temperature above 573 K although the framework structure of H-Hol is not changed by evacuation below 673 K. Since the H_2O/H^+ content in H-Hol gradually decreases with the increase of evacuation temperature (Fig. 2), the above $-\Delta H_{d,NH_3}$ behavior indicates the important role of H^+/H_2O in NH_3 adsorption on H-Hol.

Fig. 6a shows the comparison of $-\Delta H_{d,NH_3}$ at 323 and 393 K on H-Hol after evacuation at 393 and 473 K. Instead of the initial peaks at 323 K, $-\Delta H_{d,NH_3}$ curves at 393 K for both evacuation temperatures present less evident peaks with higher values at $n(NH_3) < 200$ μmol/g. $-\Delta H_{d,NH_3}$ curves at 393 K have the same shapes as those at 323 K for both evacuation temperatures in the higher NH_3 adsorption range, but demonstrate lower $-\Delta H_{d,NH_3}$ values. Fig. 6b shows the curves of the differential adsorption entropies ($-\Delta S_{d,NH_3}$) for NH_3 adsorption at both adsorption temperatures, which are calculated by the following equation:

$$\Delta S_{d,NH_3} = -R \ln\left(\frac{P}{P_0}\right) + \frac{\Delta H_{d,NH_3}}{T} \quad (1)$$

where T, P and P_0 are the adsorption temperature, NH_3 gas pressure, and saturated vapor pressure of NH_3 at T, respectively. The $-\Delta S_{d,NH_3}$ values at 393 K are smaller than those at 323 K in the whole adsorption range, indicating that the NH_3 molecules adsorbed at 393 K have more freedom of mobility than those at 323 K.

4. Discussion

The layered structure of H-Bir is constructed of the stacked MnO_6 octahedral sheets with slit-shaped micropores in between. Multialkylammonium ions can easily enter the slit-shaped micropores from the liquid phase, leading to expansion of the layered structure or even delamination if further washed with water [23]. The layered structure of H-Bir is stabilized by the included H_2O with H–bond, giving a basal spacing of 0.729 nm and a crystalline pore opening of 0.28 nm [23]. When NH_3 is inserted into the layered structure, the produced NH_4^+ ions induce attraction between two MnO sheets, giving rise to a shorter basal spacing of 0.717 nm as confirmed by XRD analysis of NH_3-adsorbed H-Bir (Table 1). All these facts indicate a flexible property of the stacked layered structure of H-Bir into which NH_3 can be easily inserted in a more mobile manner. However, inter-linking of the MnO_6 octahedral units leads to a more stable tunnel structure of H-Hol, into which the inserted NH_3 can be strongly localized. Hence, the structural difference of H-Bir and H-Hol can give the reason for the higher $-\Delta H_{d,NH_3}$ value on H-Hol but much lower $-\Delta H_{d,NH_3}$ value on H-Bir.

Fig. 7 shows the adsorption isotherms of NH_3 in the low NH_3 gas pressure range at various evacuation temperatures. NH_3 adsorption at the low NH_3 gas pressure range basically decreases with the increase

Table 1
Lattice constants of H-Hol and H-Bir before and after NH_3 adsorption

Sample	Pre-evacuation temperature (K)	Adsorption temperature (K)	Adsorption amount (μmol/g)	$a_0(b_0)$ (nm)	c_0 or d_0 (nm)
H-Hol	393	–	0	0.975 ± 0.003	0.285 ± 0.001
		323	394	0.981 ± 0.001	0.285 ± 0.001
			2189	0.985 ± 0.002	0.286 ± 0.001
		393	1632	0.986 ± 0.004	0.286 ± 0.001
	473	–	0	0.977 ± 0.001	0.286 ± 0.001
		323	315	0.979 ± 0.002	0.285 ± 0.001
			1718	0.987 ± 0.003	0.286 ± 0.001
		393	1019	0.982 ± 0.001	0.285 ± 0.001
	573	–	0	0.973 ± 0.002	0.286 ± 0.001
		323	572	0.977 ± 0.001	0.285 ± 0.001
K-Hol	393	–	0	0.979 ± 0.002	0.285 ± 0.001
	393	323	306	0.981 ± 0.001	0.285 ± 0.001
H-Bir	323	–	0	–	0.729
	323	323	1537	–	0.717

of dehydration temperature of H-Hol. Non-dehydrated H-Hol (Fig. 7a) has the highest NH_3 adsorption at low NH_3 pressure range irrespective of a lower interaction energy (Fig. 5), indicating that there exist some weakly attached H^+ or some kind of water sites at a low temperature for NH_3 adsorption. These weakly attached H^+ sites or adsorbed water will be mainly present in the external surface or near the tunnel

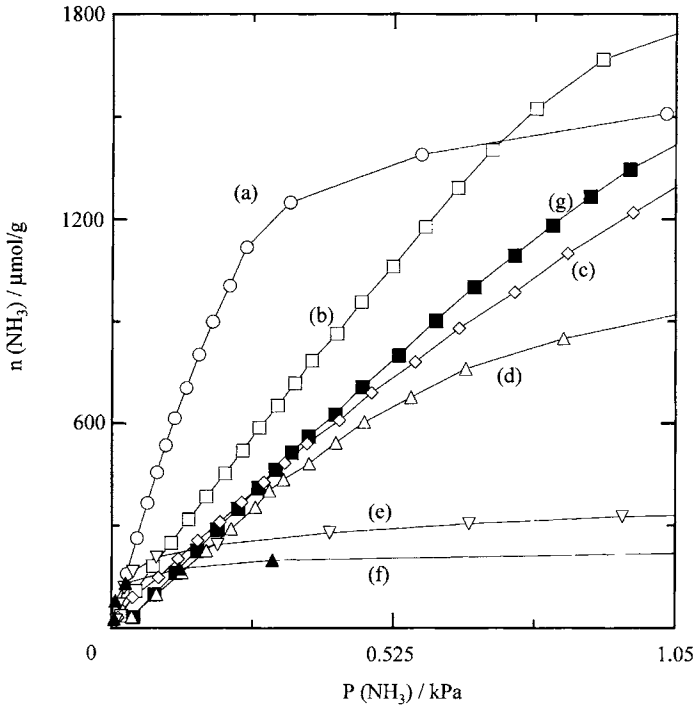

Fig. 7. NH_3 adsorption isotherms on H-Hol at 323 K after pre-evacuation at (a) 323, (b) 393, (c) 473, (d) 573, (e) 673 and (f) 773 K and at 393 K after pre-evacuation at (g) 393 K.

entrance, hindering the further access of NH_3 to the H^+ sites in the inner part of the tunnel and thus giving a smaller NH_3 adsorption amount in a higher pressure range in comparison with that on H-Hol dehydrated at 393 or 473 K. Dehydration of H-Hol at 393 and 473 K gradually leads to the disappearance of weakly attached H^+ sites and adsorbed water on the external surface, resulting in the higher $-\Delta H_{d,NH_3}$ values due to the interaction between the more exposed H^+ sites and NH_3 to form strongly localized NH_4^+ (Fig. 5).

In general, a peak or increased values in a $-\Delta H_d$ curve can often be observed for enhanced inter-molecular interaction among adsorbates at a higher adsorption [26–28]. However, this behavior can be excluded in this case because of the range of strong gas-solid interaction. Furthermore, it is unlikely that surface diffusion of a localized adspecies with an adsorption energy of 200 kJ/mol can be an obstacle to the formation of a progressively increasing $-\Delta H_{d,NH_3}$ curve at the initial NH_3 adsorption stage [29]. Because of its great ionic diameter (0.296 nm), the insertion as a form of NH_4^+ leads to expansion of the stable framework of H-Hol. Table 1 shows a comparison of lattice constants of H-Hol before and after NH_3 adsorption. The expansion of the lattice structure of H-Hol occurs even at the ending points of the peaks in $-\Delta H_{d,NH_3}$ curves at the initial NH_3 adsorption; the degree of the expansion increases with the increase of NH_3 adsorbed. Since more energy is necessary for the lattice expansion, the energy barrier to the opening of the tunnel mouth can be a greater obstacle for NH_3 insertion. Thus, the initial NH_3 insertion into the tunnel structure needs other driving forces such as a higher gas concentration or an elevated temperature, and cannot be as easy as the reaction with the remaining H^+ sites weakly attached at the external surface. For this reason, $-\Delta H_{d,NH_3}$ values at the initial NH_3 adsorption stage include two contributions: one is a lower interaction energy contribution from the reaction with the remaining H^+ sites weakly attached at the external surface; the other is a higher interaction energy contribution from NH_3 insertion into the tunnel structure near the entrance. The NH_3 molecules reach the weak H^+ sites at the external surface first and then gradually are inserted into the tunnel structure by the driving force of successively increased gas concentration, thus, forming a peak shape in the initial NH_3 adsorption stage at a lower adsorption temperature. The greater $-\Delta H_{d,NH_3}$ values before the summit of the initial peak at evacuation of 473 K (Fig. 5c) compared to those at evacuation at 393 K (Fig. 5b) can be ascribed to the lesser contribution of NH_3 adsorption on the weak H^+ sites at the external surface due to more complete dehydration. At a higher adsorption temperature, the thermodynamic rule for an exothermic equilibrium reaction [30] requires a decreased adsorption amount on the weak H^+ sites at the external surface. However, both acceleration of diffusion and an enhanced lattice vibration can make it easier for NH_3 molecules to reach the H^+ sites in the tunnel but near the entrance at a higher temperature. That is why the peak shape of the $-\Delta H_{d,NH_3}$ curve at the initial NH_3 adsorption stage becomes less evident at the adsorption temperature of 393 K for both evacuation temperatures (Fig. 6a), demonstrating a higher $-\Delta H_{d,NH_3}$ value due to a greater contribution from the insertion reaction.

After expanding the tunnel structure by forming NH_4^+ at the initial stage, NH_3 molecules become accessible to the H^+ sites in the inner part of the tunnel, forming a secondary broad insertion stage. It should be mentioned that the insertion of NH_3 into the inner H^+ sites is a rate-determining process due to the difficulty in intra-pore diffusion. The heat-flux curves corresponding to the secondary insertion stage, which were observed in calorimetric measurement results, gave longer tailings in contrast to those for the initial adsorption stages, which have sharp peaks with almost no tailing. This secondary insertion stage is evident at a pre-evacuation condition of 393 K, but less evident at that at 473 K because of loss of inner H^+ at higher evacuation temperature. Furthermore, in line with the thermodynamic rule of an exothermic reaction, there is a lesser amount of NH_3 insertion at a higher temperature as shown in Fig. 7. For this reason, the secondary stage of NH_3 insertion becomes less evident at a higher insertion temperature (393 K). With regard to the initial peak in $-\Delta H_{d,NH_3}$ curve on K-Hol, basically the same mechanism as that on H-Hol is likely because of the small amount of H^+/H_2O existing in K-Hol, as shown in Fig. 2. NH_3 can be adsorbed on the H^+ sites at the external surface and inserted in a small amount into the tunnel structure near the entrance, but cannot be inserted into the inner part of the tunnel due to the obstacle of K^+. The expansion of the lattice structure of K-Hol due to NH_4^+ having a

larger ionic size than K^+ can also be observed from Table 1, though the expansion degree is too small to be outside the range of error because of the limited amount of NH_4^+.

5. Conclusion

1. H-Bir has a smaller $-\Delta H_{d,NH_3}$ value compared to H-Hol because of the structural flexibility of its MnO sheets.
2. At dehydration below 473 K, NH_3 insertion into the tunnel structure of H-Hol can be divided into two stages. In the initial stage, NH_3 molecules interact with the H^+ sites at the external surface and near the tunnel entrance, giving a peak in $-\Delta H_{d,NH_3}$ curve at a low temperature due to the energy barrier required to expand the lattice structure. In the secondary stage, NH_3 can access the inner H^+ sites in the tunnel, giving a broad shoulder in $-\Delta H_{d,NH_3}$ curve. H_2O/H^+ contents in H-Hol have an important role in NH_3 insertion.
3. $-\Delta H_{d,NH_3}$ values on porous manganese oxides are comparable with or much higher than those on zeolites having a similar pore dimension or of the same proton type.

References

[1] S. Bach, J.P. Pereira-Ramos, N. Baffier, Solid State Ionics 80 (1995) 151.
[2] M.H. Rossouw, D.C. Liles, M.M. Thackeray, Mater. Res. Bull. 27 (1992) 221.
[3] Y. Shao-Horn, S.A. Hackney, C.S. Johnson, M.M. Thackeray, J. Electrochem. Soc. 145 (1998) 582.
[4] T. Ohzuku, M. Kitagawa, K. Sawai, T. Hirai, J. Electrochem. Soc. 138 (1991) 360.
[5] M. Tsuji, M. Abe, Bull. Chem. Soc. Jpn. 58 (1985) 1109.
[6] M. Tsuji, M. Abe, Solv. Ext. Ion Exch. 2 (1984) 253.
[7] Y. Tanaka, J. Porous Mater. 2 (1995) 135.
[8] Q. Feng, H. Kanoh, Y. Miyai, K. Ooi, Chem. Mater. 7 (1995) 148.
[9] R.N. De Guzman, Y. Shen, B.R. Shaw, S.L. Suib, C. O'Young, Chem. Mater. 5 (1993) 1395.
[10] S.L. Brock, N. Duan, Z. Tian, O. Giraldo, H. Zhou, S.L. Suib, Chem. Mater. 10 (1998) 2619.
[11] B. Dhandapani, S.T. Oyama, Chem. Lett. (1995) 413.
[12] W.S. Kijlstra, D.D. Brands, E.K. Poels, A. Bliek, J. Catal. 171 (1997) 208.
[13] S.B. Kanungo, J. Catal. 58 (1979) 419.
[14] T. Yamashita, M.A. Vannice, J. Catal. 163 (1996) 158.
[15] L.S. Singoredjo, R.B. Korver, F. Kapteijn, J.A. Moulijn, Appl. Catal. B: Environ. 1 (1992) 297.
[16] S. Tezuka, Z.-M. Wang, K. Ooi, H. Kanoh, in: D.D. Do (Ed.), Adsorption Science & Technology, World Scientific, Singapore, 2000, p. 319.
[17] Z.-M. Wang, S. Tezuka, H. Kanoh, Chem. Lett. (2000) 560.
[18] Z.-H. Liu, K. Ooi, H. Kanoh, W. Tang, T. Tomida, Chem. Lett.(2000) 390.
[19] M.H. Rossouw, D.C. Liles, M.M. Thackeray, Mater. Res. Bull. 27 (1992) 221.
[20] D.W. Breck, Zeolite Molecular Sieves — Structure, Chemistry, and Use, Wiley/Interscience, New York, 1974.
[21] JCPDS-ICDD Powder Diffraction File no. 20-908.
[22] Z.-M. Wang, S. Tezuka, H. Kanoh, Chem. Mater. 13 (2000) 530.
[23] Z.-H. Liu, K. Ooi, H. Kanoh, W. Tang, T. Tomida, Langmuir 16 (2000) 4154.
[24] R.L. David (Ed.), Handbook of Chemistry and Physics, 76th Edition, CRC Press, Boca Raton, FL, pp. 6–116.
[25] K. Tsutsumi, K. Nishimiya, Thermochim. Acta 143 (1989) 299.
[26] H. Thamm, J. Phys. Chem. 92 (1988) 193.
[27] K. Tsutsumi, K. Mizoe, Colloids Surf. 37 (1989) 29.
[28] Z.-M. Wang, K. Kaneko, J. Phy. Chem. 99 (1995) 16714.
[29] N. Cardona-Martinez, J.A. Dumesic, Adv. Catal. 38 (1992) 149.
[30] P. Cainiti, A. Gervasini, A. Auroux, J. Catal. 150 (1994) 274.